



Correlation between lead isotope analysis and solid-state electrochemistry for determining the provenance of archaeological bronze

Antonio Doménech-Carbó¹ · Joan Bernabeu-Aubán²

Received: 29 June 2019 / Revised: 22 August 2019 / Accepted: 24 August 2019 / Published online: 5 September 2019
© Springer-Verlag GmbH Germany, part of Springer Nature 2019

Abstract

The voltammetry of microparticles (VIMP) methodology was applied to a set of submicrosamples from the corrosion layers of copper artifacts from the archaeological site of La Vital (Gandia, Spain), dated back to 4200 to 3900 BP, attached to graphite electrodes in contact with aqueous acetate buffer at pH 4.50. Signals for the reduction of cuprite plus malachite, dominating the composition of the corrosion layers, and tenorite, were used for grouping the samples. A model to describe their relative concentrations assuming gradients following a potential law is proposed and tested with experimental data. Correlation of VIMP sample grouping with lead isotope data in literature permitted to discriminate archaeological samples depending on the provenance of raw materials and the manufacturing process.

Keywords Electrochemistry · Archaeometry · Metal provenance · Isotope analysis · Corrosion products

Introduction

The determination of the geographical origin of raw materials, mining activities, manufacturing technology, chronology, and/or trade routes is common targets in the study of archaeological objects made of metals [1, 2]. The chemical composition and metallographic structure are important analytical targets for which different techniques have been applied [3, 4], usually combined in multi-technique approaches [5, 6]. In particular, isotope analysis from inductively coupled plasma-mass spectrometry (MC-ICP-MS) technique has emerged as a very

powerful tool for these purposes, lead [7–10] and, to a lesser extent, copper [11, 12], being the elements usually used to study several archeological metals.

Several of these techniques require a more or less extensive sampling within the metal core. As far as deep sampling is not allowed or seriously restricted for archaeological artifacts, there is a continuous interest in developing non-invasive or minimally invasive techniques [13, 14]. This implies that the archaeometric information has to be derived from the analysis of the physicochemical properties of the metal patina of corrosion [15–17].

In this context, the voltammetry of immobilized particles (VIMP), a solid-state electrochemical methodology developed by Scholz et al. [18–20], has been applied to the study of metal patinas [21–25]. The interest of this technique derives from its high sensitivity and its requirement of amounts of sample at the sub-microgram level which make it minimally invasive, prompting its application for archaeometry, conservation, and restoration, as described in different reviews [26–29]. In particular, the VIMP has been recently applied for discriminating between different monetary emissions of silver [30–32] and bronze/copper [33–36] coins and dating copper/bronze [37, 38], lead [39], and gold [40–42] archaeological objects, as recently revised [43]. Archaeometric applications of VIMP combined with electrochemical impedance spectroscopy (EIS) have been also reported [44–46].

Electronic supplementary material The online version of this article (<https://doi.org/10.1007/s10008-019-04378-3>) contains supplementary material, which is available to authorized users.

✉ Antonio Doménech-Carbó
antonio.domenech@uv.es

✉ Joan Bernabeu-Aubán
joan.bernabeu@uv.es

¹ Departament de Química Analítica, Universitat de València, Dr. Moliner, 50, 46100 Burjassot, València, Spain

² Grupo PREMEDOC, Departament de Prehistoria, Arqueologia i Historia Antiga, Universitat de València, Blasco Ibañez, 28, Passeig al Mar s/n, València, Spain

Here a study correlating the grouping of archaeological samples is reported using VIMP with prior analytical data using X-ray fluorescence spectroscopy (XRF), scanning electron microscopy (SEM), and lead isotope analysis [47] on a series of bronze objects from the site of La Vital (Gandia, Spain). This archaeological site is particularly interesting because it presents the first evidences for copper metallurgy in the Iberian Peninsula [47, 48]. From the 14 radiocarbon dates obtained, we can assume a time span ranging from ca. 4200 to 3900 cal. BP [48]. This includes from the beginning of the Chalcolithic to the Bell Beaker period. Copper metallurgy is present from the beginning, including melting pots, metallurgical waste, and tools. The location of the site, next to the mouth of the Serpis river, gives it a special importance in investigating the supply routes for copper ore, absent in the region.

Although lead isotope analysis offers difficulties derived from the use of additives and/or ore mixtures, the reuse of the metals, isotope fractionation during ore processing and manufacturing of the objects, and environmental paleocontamination [49–51], this technique can be considered as a logical reference for validating studies on the provenance and distribution of archaeological objects. Specifically, the idea is to contrast the provenance data derived from lead isotope analysis with the minimally invasive VIMP analysis of the patinas of the objects.

Experimental

Samples

A set of 8 objects from La Vital site were studied (see Table 1). These were three residues of metallurgical activities and 5 tools (one ax, one chisel, one dagger, and two awls). All of them were analyzed using XRF, SEM, and lead isotope analysis, and parallel radiocarbon dating of organic residuals was available [48].

Instrumentation and methods

Electrochemical experiments were performed at 298 K in air-saturated aqueous 0.25 M sodium acetate buffer (Panreac) at pH 4.75 using a three-electrode cell connected to a CH I660C potentiostat (Cambria Scientific, Llwynhendy, Llanelli, UK). The electrolyte was renewed after each electrochemical run to avoid contamination due to metal ions eventually released to the solution phase during electrochemical turnovers. To test the possibility of using portable equipment, no deaeration was performed. Square wave voltammograms (SWVs) and cyclic voltammograms (CVs) were obtained on sample-modified graphite electrodes, a platinum wire counterelectrode, and an Ag/AgCl (3 M NaCl) reference electrode completing the three-electrode arrangement.

Sampling was performed with commercial paraffin-impregnated graphite bars (Alpino, HB type, 2.0 mm diameter) by pressing and lightly rotating it onto a region of the sample surface during ca. 5 s. One, two, or three samples were taken for each coin depending on the availability of regions of uniformly hued surface. VIMP for reference materials was carried out using conventional VIMP protocols [18, 19] by powdering an amount of 1–2 mg of the solid in an agate mortar and pestle, and extending it on the agate mortar forming a spot of finely distributed material. Then, the lower end of the graphite electrode was gently rubbed over that spot of sample and finally rinsed with water to remove ill-adhered particles. Sample-modified graphite bars were then dipped into the electrochemical cell so that only the lower end of the electrode was in contact with the electrolyte solution.

The IR spectra in the ATR mode of the samples were obtained using a Vertex 70 (Bruker Optik GmbH, Germany) Fourier-transform infrared spectrometer with an FR-DTGS (fast recovery deuterated triglycine sulfate) temperature-stabilized coated detector and an MKII Golden Gate attenuated total reflectance (ATR) accessory. A total of 32 scans were collected at a resolution of 4 cm⁻¹ and the spectra were processed using the OPUS 5.0/IR software (Bruker Optik GmbH, Germany).

Table 1 Description of the samples from La Vital archaeological site and reported age from radiocarbon analysis of accompanying organic materials [44, 45]

Sample	Description	²⁰⁷ Pb/ ²⁰⁶ Pb	Isotopic type	Radiocarbon age	Ag (wt%)	As (wt%)
PA12342	Burr	0.841	C	4180 ± 50 BP	0.124	0.25
PA12487	Awl	0.839	B	Unavailable	0.239	1.8
PA12489	Chisel	0.842	C	Unavailable	0.124	b.l.
PA12491	Ax	0.847	D	3959 ± 24 BP	0.147	0.38
PA12492	Awl	0.853	D	3959 ± 24 BP	0.129	0.14
PA12471	Sphaerule	0.849	D	4040 ± 40 BP	0.168	b.l.
PA12475	Sphaerule	0.837	A	4040 ± 40 BP	0.187	0.93
PA12473	Dagger	Unavailable		3830 ± 40 BP	0.272	1.78

Results and discussion

Age, composition of the metal core, and corrosion products

The studied samples presented a uniform green patina, often locally darker, indicative of a relatively advanced but homogeneous corrosion under burial conditions. The infrared spectra (see Fig. 1) was dominated by the bands due to the carbonate group at 1391, 868, and 713 cm^{-1} , denoting the presence of malachite as a main corrosion product accompanied by calcite and clayey minerals, identified by their absorption bands of Si-O group at 1020 (shoulder) and 1006 cm^{-1} . Weak cuprite (630 cm^{-1}) and tenorite 620 cm^{-1}) bands were also recorded. Such copper corrosion products display weak infrared signals [52, 53] but their presence is consistent with the usual corrosion scheme consisting of a primary patina of cuprite further developing a secondary patina where this mineral is progressively replaced by other corrosion products [14].

The analysis of the metal core revealed a high content of Cu (98–100 wt%) accompanied by low amounts of As (below 1.8 wt%), Pb (below 1 wt%), and Ag (between 0.12 and 0.24 wt%) [47]. Four samples were suitable for ^{14}C dating. The age of sample PA12473 was estimated as 3830 ± 40 BP and that of samples PA12491 and PA12492 was estimated as 3959 ± 24 BP (the date is a mean of two radiocarbon dates obtained from the same burial bone); samples PA12471 and 12475 come from the same pit dated in 4040 ± 40 BP. These two dates could be statistically of the same age. On the other side, sample PA 12342 could be earlier according with the radiocarbon date obtained from a neighbor pit (4180 ± 50 BP). And finally, the dagger (sample PA12473) could be the most recent documented at the site. It comes from a burial associated with a Bell Beaker pot. Such data are provided as a Supplementary information (Table S.1) [48].

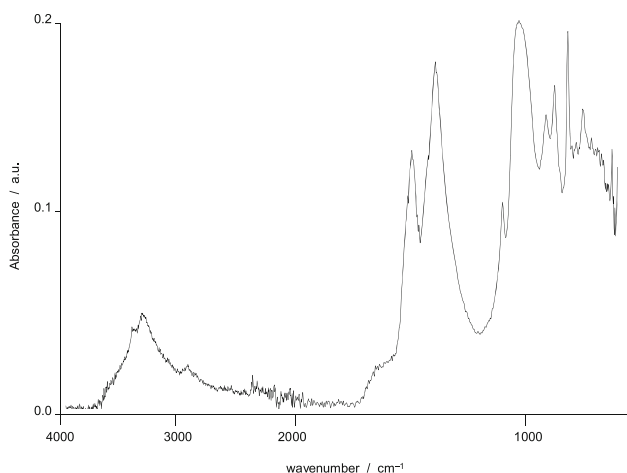


Fig. 1 ATR-FTIR spectrum of sample PA12487

Lead isotope analysis

Reported data of the lead isotope analysis of the studied samples are summarized in Supplementary information, Table S.2 [47]. Correlation with data for minerals of mines in the SE region of Iberia led to attribute sample PA12475 to ALCOLEA 6 mine; PA12471 to an unknown mine, but in the SE of Iberia; and PA12487 probably to the Almizaraque area, once again in the SE of Iberia [47]. Figure 2 depicts the plots of (a) $^{208}\text{Pb}/^{206}\text{Pb}$ vs. $^{207}\text{Pb}/^{206}\text{Pb}$ and (b) $^{206}\text{Pb}/^{204}\text{Pb}$ vs. $^{207}\text{Pb}/^{206}\text{Pb}$ for the studied La Vital samples. One can see that, in agreement with results for other systems in the Mediterranean area [54, 55], data points for the studied samples fall within the diagonals of the diagrams in both representations. The studied samples can be grouped in the same four sectors labeled as follows: group A: sample P12475; group B: sample PA12487; group C: samples PA12342 and PA12489; and group D: samples PA12471, PA12491, and PA12492.

On comparing the above grouping with elemental composition data, one can see that, as depicted in Fig. 3a, where the

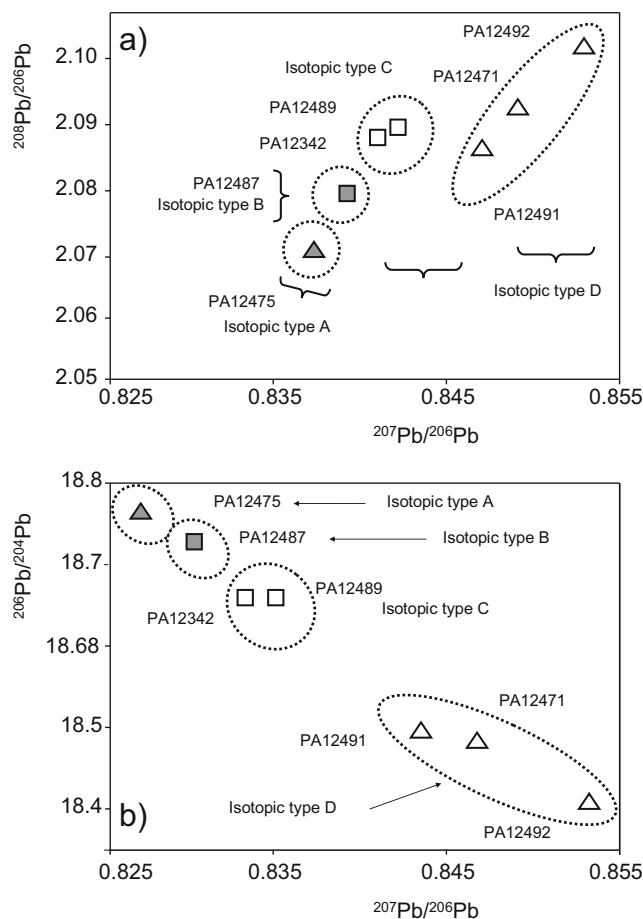


Fig. 2 Plots of **a** $^{208}\text{Pb}/^{206}\text{Pb}$ vs. $^{207}\text{Pb}/^{206}\text{Pb}$ and **b** $^{206}\text{Pb}/^{204}\text{Pb}$ vs. $^{207}\text{Pb}/^{206}\text{Pb}$ for samples in this study from data in [44]

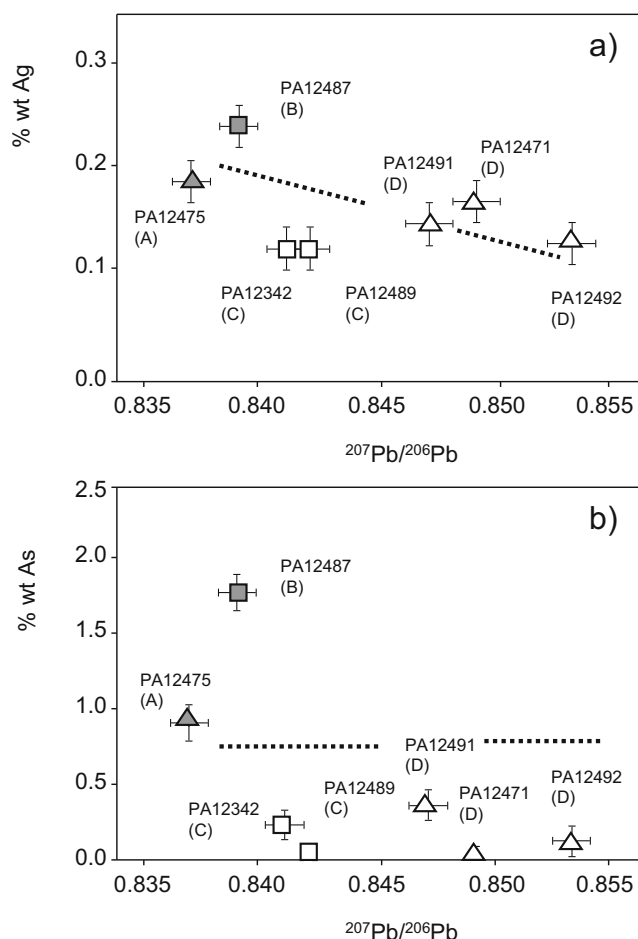


Fig. 3 Plots of **a** the percentage of Ag and **b** the percentage of As in the metal core of La Vital samples vs. the $^{207}\text{Pb}/^{206}\text{Pb}$ isotopic ratio from data in [44]

percentage (wt%) of Ag is plotted vs. the $^{207}\text{Pb}/^{206}\text{Pb}$ ratio, it appears that, although the Ag content is constrained to a narrow range, there is a certain correlation between the two quantities. As far as, in contrast to As and Sb (vide infra), Ag is not significantly released during the manufacturing of objects, the above data suggest that the raw materials proceed from different sources from a relatively restricted geographical area.

Figure 3 b shows a representation of the percentage (wt%) of As vs. the $^{207}\text{Pb}/^{206}\text{Pb}$ ratio. Here, there is a sharp contrast between samples of the isotopic types A and B, having relatively high As contents, and samples of the types C and D, all with As contents below 0.5 wt%. Similar results were obtained for the Sb content. Since both elements experience loss by thermal stress, their low contents in samples C and D can be considered as indicative of the recycling of metal objects. Interestingly, sample PA12473 for which there are no available lead isotope data was characterized by As and Sb contents close to those of sample PA12487, ascribed to the isotopic type B (see Table 1). This coincidence, treated in detail below, suggests a common source of the raw materials.

Voltammetric pattern

Figure 4 depicts the square wave voltammograms (three replicate experiments) for submicrosamples from the corrosion layer of PA12489 attached to graphite electrodes in contact with air-saturated 0.25 M aqueous acetate buffer at pH 4.50. Upon scanning the potential from +1.25 V vs. Ag/AgCl in the negative direction, a main cathodic peak appears at -0.10 V vs. Ag/AgCl (C_{Cu1}) which is followed by a shoulder at -0.30 V (C_{Cu2}) and a wave peaked at -0.70 V (C_{ox}) with a shoulder at ca. -0.55 V (C_{Pb}). Upon scanning the potential from -1.05 V in the positive direction, a sharp anodic signal appears at 0.0 V (A_{Cu}), often exhibiting some degree of peak splitting, preceded by a shoulder at -0.50 V (A_{Pb}). At the negative and positive extreme potentials, the rising currents for the hydrogen evolution reaction (HER) and oxygen evolution reaction (OER) respectively appear. This voltammetric response can be interpreted on the basis of abundant literature on the electrochemistry of copper and lead corrosion products so that the peak C_{Cu1} can be attributed to the reduction of cuprite (Cu_2O) superimposed to the reduction of copper corrosion products of minerals of the malachite, brochantite, and/or atacamite families [21–25]. The signal C_{Cu2} corresponds to the reduction of tenorite (CuO) [32–36] whereas the signal C_{Pb} corresponds to the reduction of lead corrosion products, mainly litharge accompanied by minerals of the anglesite and cerussite families [38, 56]. The cathodic signal C_{ox} can be attributed to the

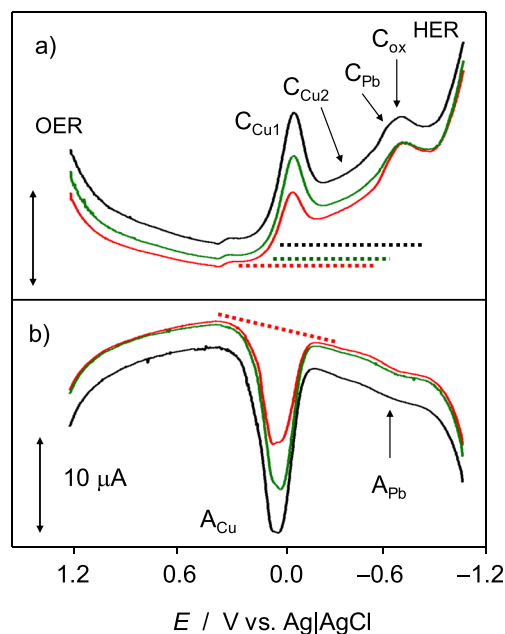


Fig. 4 Square wave voltammograms (three replicate experiments) for submicrosamples from the corrosion layer of PA12489 attached to graphite electrodes immersed into air-saturated 0.25 M HAc/NaAc, pH 4.50. Potential scan initiated at **a** +1.25 V in the negative direction and **b** -1.05 V in the positive direction. Potential step increment 4 mV, square wave amplitude 25 mV, frequency 5 Hz. The dotted lines represent the baselines used for peak current measurements

reduction of dissolved oxygen, a well-known electrochemical process. In the positive-going potential scan voltammograms, the peaks A_{Pb} and A_{Cu} correspond to the oxidative dissolution of the deposits of Pb and Cu metals electrochemically formed in the reduction of the corrosion products.

Modeling corrosion pattern

As can be seen in Fig. 4, replicate sampling on the same object produces similar but not identical voltammograms. This feature obeys, as previously described, to the abrasive nature of the sampling process, which results in the transference of variable amounts of corrosion products to the electrode surface. The measurement of peak currents for the signals C_{Cu1} , C_{Cu2} , A_{Pb} , and A_{Cu} was made using the baselines depicted in Fig. 4 taking the corresponding maximum in the current/potential curve. This criterion was adopted based on the existence of small peak potential shifts (less than 15–20 mV) obtained in replicate experiments on the same sample. These can be attributed, as already discussed [56], to the different uncompensated ohmic drops associated with the different net amounts of nonconducting metal corrosion products transferred onto the graphite electrode surface.

Measurement of the peak currents (i) for the processes C_{Cu1} and C_{Cu2} indicated that the peak current ratio, $i(C_{Cu2})/i(C_{Cu1})$, decreased on increasing the absolute value of the current $i(C_{Cu1})$ resulting in $i(C_{Cu2})/i(C_{Cu1})$ vs. $i(C_{Cu1})$ plots such as in Fig. 5a, corresponding to the entire set of objects of La Vital site grouped by isotopic types. Fit of experimental data to a potential law yields clearly separated curves for each one of the isotopic types. Within each isotopic type, the different samples provide essentially coincident tendency lines, as can be seen in Fig. 5b for samples of type D.

This variation can be interpreted taking into account that the $i(C_{Cu2})/i(C_{Cu1})$ ratio represents the quotient between the amounts of tenorite and the sum of cuprite and malachite existing in the sampled corrosion layer. Since the total amount of these components will depend on the penetration of the graphite bar in the corrosion layers, the observed variation of $i(C_{Cu2})/i(C_{Cu1})$ on $i(C_{Cu1})$ can be interpreted as representative of a gradient in the concentration of the different corrosion products.

This interpretation is consistent with the recognized nature of copper and bronze corrosion in burial environments. Here, the corrosion proceeds via formation of a primary patina of cuprite further forming a secondary patina where cuprite is accompanied by other corrosion products, usually of the families of malachite, atacamite, and/or brochantite [14]. The formation of tenorite from cuprite is a thermodynamically spontaneous process whose occurrence is favored by the contact with an O_2 -rich atmosphere and/or carbonate-rich environments [57]. This means that the proportion of tenorite in the corrosion layers will increase from deeper to surface corrosion

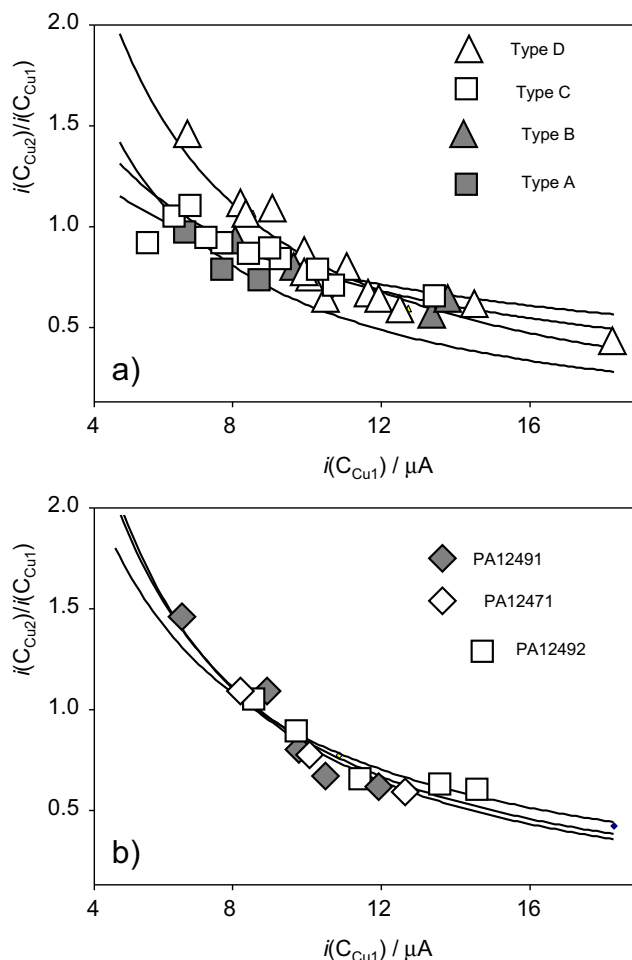


Fig. 5 Variation of the $i(C_{Cu2})/i(C_{Cu1})$ current ratio on $i(C_{Cu1})$ for **a** the entire set of objects of La Vital site grouped by isotopic types and **b** the individual samples of the isotopic type D. Data points from 3–5 replicate voltammograms such as in Fig. 4 for each sample. Continuous lines represent the curves resulting from the fit of experimental data to a potential law for each sample. Error bars are omitted for clarity

layers so that opposite concentration gradients of cuprite and tenorite will appear in the corrosion layers of coins, as already described [32–36].

However, in contrast with previously studied systems, constituted by moderately corroded series of copper/bronze coins [32–36], the archaeological artifacts studied here contain a uniform, but relatively gross secondary patina mainly formed by malachite. Accordingly, one can model differently this system in terms of the formation of a primary patina of cuprite (where there is, presumably, a gradient of crystallinity and hydration degree) giving rise, in a process driven by O_2 plus H_2O diffusion, to the formation of a secondary patina with a competitive formation of tenorite and malachite, as schematized in Fig. 6. Then, the number of tenorite grains per volume unit in the secondary patina, n_{ten} , and the corresponding quantity for malachite grains, n_{mal} , can be assumed to increase from 0 in the primary/secondary patina boundary, located at a deep

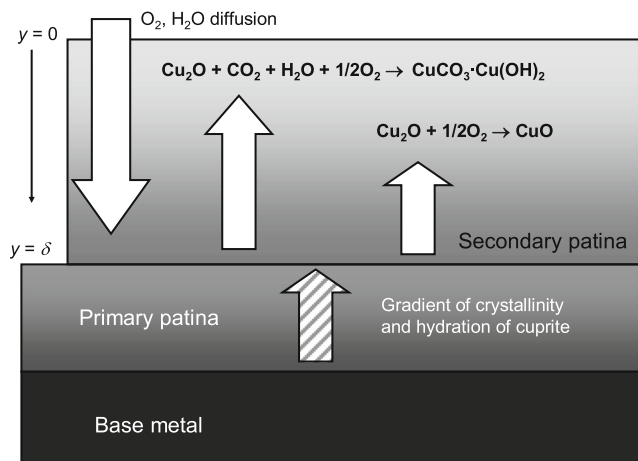


Fig. 6 Scheme for modeling corrosion of copper objects in this study

$y = \delta$ to values n_{ten}^{sup} and n_{mal}^{sup} at the external surface of the secondary patina ($y = 0$), whereas the number of grains per volume unit of cuprite, n_{cup} , will decrease from its value in the primary patina n_{cup}^o to a surface value of n_{cup}^{sup} . Assuming that the formation of secondary corrosion products follows competing potential rate laws, introducing a non-dimensional depth, $z = 1 - y/\delta$, one can write:

$$n_{ten} = n_{ten}^{sup} z^\alpha \tag{1}$$

$$n_{mal} = n_{mal}^{sup} z^\beta \tag{2}$$

$$n_{cup} = n_{cup}^o - (n_{ten}^{sup} z^\alpha + n_{mal}^{sup} z^\beta) \tag{3}$$

When a graphite bar of section S is pressed onto the corrosion layers of an object, a net volume V of corrosion products was transferred to the electrode surface so that, ideally, $V = bSz$, where z denotes the depth reached in the sampling and b reflects the adherence of the material forming the corrosion layers. Since the currents measured in VIMP experiments can be considered as proportional to the total number of respective grains adhered to the graphite bar, the peak area or (peak current) of the signal C_{Cu1} (cuprite plus malachite) and C_{Cu2} (tenorite) can be written as:

$$i(C_{Cu2}) = \int_0^z \epsilon_{ten} n_{ten} dV = \int_0^z b_{ten} \epsilon_{ten} n_{ten}^{sup} S z^\alpha dz \tag{4}$$

$$i(C_{Cu1}) = \int_0^z (\epsilon_{cup} n_{cup} + \epsilon_{mal} n_{mal}) dV = \int_0^z \left\{ b_{cup} \epsilon_{cup} \left[n_{cup}^o - (n_{ten}^{sup} z^\alpha + n_{mal}^{sup} z^\beta) \right] + b_{mal} \epsilon_{mal} n_{mal}^{sup} z^\beta \right\} S dz \tag{5}$$

where ϵ_{ten} , ϵ_{cup} , and ϵ_{mal} represent electrochemical constants characterizing the reduction processes of tenorite,

cuprite, and malachite to copper metal. These constants depend on the electrochemical conditions (electrolyte, temperature, potential scan rate, etc.). Integration of Eqs. (4) and (5) yields:

$$i(C_{Cu2}) = \frac{b_{ten} \epsilon_{ten} S n_{ten}^{sup}}{1 + \alpha} z^{1+\alpha} \tag{6}$$

$$i(C_{Cu1}) = b_{cup} \epsilon_{cup} S \left[n_{cup}^o z - \frac{n_{ten}^{sup} z^{1+\alpha}}{1 + \alpha} \right] + (b_{mal} \epsilon_{mal} - b_{cup} \epsilon_{cup}) \frac{n_{mal}^{sup} z^{1+\beta}}{1 + \beta} \tag{7}$$

Under our experimental conditions, malachite is the largely prevailing component of the secondary patina, so that one can approximate:

$$i(C_{Cu1}) \approx S b_{mal} \epsilon_{mal} \frac{n_{mal}^{sup} z^{1+\beta}}{1 + \beta} \tag{8}$$

$$\frac{i(C_{Cu2})}{i(C_{Cu1})} \approx \frac{(1 + \beta)^{1+\alpha-\beta} b_{ten} \epsilon_{ten} n_{ten}^{sup}}{(1 + \alpha) S^{\alpha-\beta} b_{mal}^{1+\alpha-\beta} \epsilon_{mal}^{1+\alpha-\beta} (n_{mal}^{sup})^{1+\alpha-\beta}} i(C_{Cu1})^{\alpha-\beta} \tag{9}$$

This equation predicts a potential variation of the of $i(C_{Cu2})/i(C_{Cu1})$ ratio on $i(C_{Cu1})$.

Using the same type of graphite bar and identical electrochemical conditions of experimentation, S and the ϵ , b terms will be the same for each series of samples, but the parameters n_{ten}^{sup} , n_{mal}^{sup} , α , and β will be dependent on the characteristics of the corrosion layer, in turn depending on the composition of the base metal, its metallographic structure, and the “corrosion history” of the artifact.

Correlation between isotope analysis and voltammetric data

The series of objects studied here were characterized by the following: (i) the uniformity of the base metal composition (98–100 wt% Cu) [47]; (ii) the apparent uniformity of the corrosion process and the relative similarity in the age (the dated objects cover a period between 3830 ± 40 and 4180 ± 50 BP years) [48]. In these circumstances, although there is no expectance, in view of the low Pb content in the base metal composition, of a direct influence of the isotopic composition of lead in the electrochemical response, it is reasonable to expect that the differences in the chemical composition of the raw materials and the manufacturing process will be reflected in textural differences in the produced metallic

material, in turn resulting in differences in the voltammetric response of objects submitted to a common “corrosion history,” as evidenced in silver [30–32] and bronze [33–36] coins.

Consistently with the foregoing set of considerations, plots of $\log[i(C_{Cu2})/i(C_{Cu1})]$ vs. $\log i(C_{Cu1})$ for the studied samples were grouped along straight lines, as depicted in Fig. 7. This figure indicates that there is a regular variation of such parameters, thus suggesting that the values of the slope (equal to $\alpha - \beta$, according to Eq. (9)) are related to those of the n_{ten}^{sup} and n_{mal}^{sup} values, consistently with the idea that all these parameters define the characteristics of the corrosion response of the object in turn depending on the composition of the raw material and the type of metallurgical processing.

The statistical parameters for the regression analysis applied to $\log[i(C_{Cu2})/i(C_{Cu1})]$ vs. $\log i(C_{Cu1})$ plots are summarized in Table 2. In order to test the possibility of an electrochemical grouping similar to the isotopic grouping, the slopes and ordinates at the origin of the above representations were used to construct the two-dimensional diagram in Fig. 8. Remarkably, data points for isotopic types A, C, and D defined straight lines with different slopes and ordinates at the origin so that the electrochemical grouping illustrated in Fig. 8 becomes clearly similar to the isotopic grouping depicted in Fig. 2 a and b. Comparison of such data with isotope ratios and elemental composition indicates:

(a) Samples of the isotopic type C, from a burr and a chisel characterized by low As and Sb contents, also present a common electrochemical pattern, thus suggesting the use of a similar raw material and manufacturing procedure. Then, it appears reasonable to conjecture that the age of sample PA12489, for which no ^{14}C data were available, was similar to that of sample PA12342 (4180 ± 50 BP).

Table 2 Statistical parameters for the fit to a potential law of $\log[i(C_2)/i(C_1)]$ vs. $\log i(C_1)$ straight lines for the studied series of individual La Vital samples as well as joining the data points for the objects isotopic types C and D. N represents the number of data points corresponding to sampling in different spots on the archaeological object

Series	N	Ordinate at the origin	Slope	r
Isotopic type A				
PA12475	5	(0.88 ± 0.04)	-1.09 ± 0.05	0.996
Isotopic type B				
PA12487	5	(0.57 ± 0.11)	-0.67 ± 0.11	0.98
Isotopic type C				
PA12489	12	(0.52 ± 0.05)	-0.62 ± 0.06	0.96
PA12489	8	(0.53 ± 0.05)	-0.62 ± 0.05	0.97
PA12342	4	(0.6 ± 0.3)	-0.6 ± 0.3	0.70
Isotopic type D				
PA12471	4	(1.12 ± 0.19)	-1.21 ± 0.19	0.96
PA12491	7	(1.05 ± 0.09)	-1.13 ± 0.10	0.98
PA12492	5	(0.90 ± 0.16)	-0.97 ± 0.15	0.95
Isotopic type unknown				
PA12473	3	(0.74 ± 0.04)	-0.60 ± 0.03	0.998

(b) Although having low As and Sb contents, there were differences in the age and chemical composition of samples of the isotopic type D. Presumably, such samples used similar raw materials (as suggested by the similar isotopic composition) but the objects were manufactured in different times and ages (3959 ± 24 BP for samples BP12491 and P12492, and 4040 ± 40 BP for sample PA12471). Consistently, these samples occupied a position clearly separated from the above group in the diagram in Fig. 8 but having separations in their positions in that diagram.

(c) The data point in the electrochemical diagram of sample PA12487, which corresponds to the isotopic type B, was close to that of the isotopic type C. As far as the isotopic

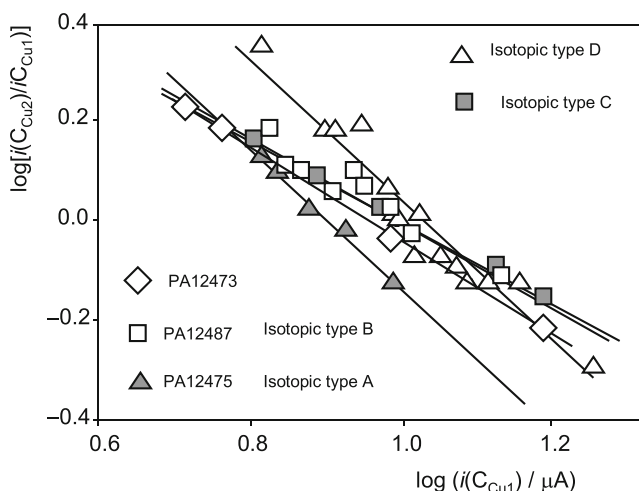


Fig. 7 Variation of $\log[i(C_{Cu2})/i(C_{Cu1})]$ on $\log i(C_{Cu1})$ for La Vital samples under study from voltammetric data in the conditions such as in Fig. 4

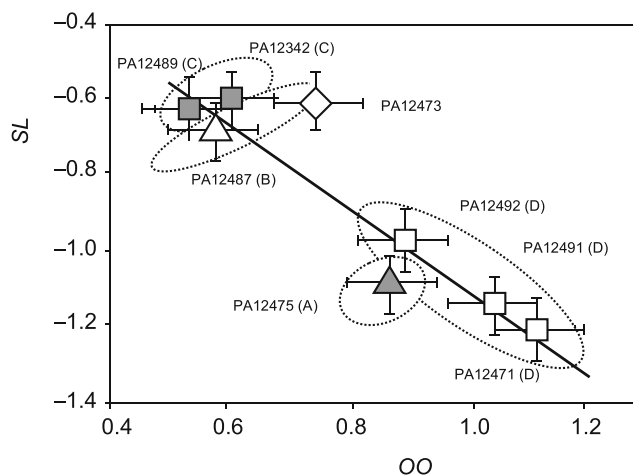


Fig. 8 Variation of the slope (SL) of the $\log[i(C_{Cu2})/i(C_{Cu1})]$ vs. $\log i(C_{Cu1})$ linear representations on the ordinate at the origin (OO) of the same for La Vital samples

and chemical composition of PA12487 was clearly different to C samples, the electrochemical similarity suggests that this object, although using a different raw material, was manufactured using a metallurgical methodology similar to that used in the production of samples PA12432 and PA12489.

- (d) The position of sample PA12473, whose isotopic composition was unavailable, was close to that representative of sample PA12487 (isotopic type B). Given the coincidence in the Ag, As, and Sb composition and the electrochemical response (see Tables 1 and 2), it appears reasonable to conjecture that both samples used a similar raw material and undergo similar manufacturing procedure and possibly age.
- (e) The object of the isotopic type A, PA12475, produced a clearly different straight line in the $\log[i(C_{Cu2})/i(C_{Cu1})]$ vs. $\log i(C_{Cu1})$ representation. The slope of the corresponding straight line was similar to that defined for the objects of the isotopic type C but the ordinate at the origin was clearly different. As far as sample PA12475 was a sphaerule similar to PA12471, it appears reasonable to identify these objects as remainings of the metallurgical process so that sample PA12475 would have been produced similarly to samples of the isotopic type D but using a raw material of different provenance.

This last hypothesis would be consistent with the chronological distribution of the sources of raw materials depicted in Fig. 9. On studying the variation of the $^{209}\text{Pb}/^{204}\text{Pb}$ ratio, representative of the isotopic type, on the radiocarbon age (Fig. 9a), one can see that the oldest samples (PA12342 and PA12489) corresponded to the isotopic type D. Apparently, this source was replaced in the next period (roughly, between 3900 and 4100 BP) by two other sources, corresponding to the isotopic types A and C. Finally, after ca. 3900 BP, samples PA12473 and PA12487, which can be considered on the basis of chemical composition and electrochemical data as made from the same raw material and age (3830 ± 40 BP), defined the isotopic type B, thus suggesting that different sources were successively used in the studied period. This scheme appears to be similar to that depicted in Fig. 9b where the slope of the $\log[i(C_{Cu2})/i(C_{Cu1})]$ vs. $\log i(C_{Cu1})$ linear representations was correlated to the radiocarbon age of the samples. Again, samples of the isotopic types A and D become grouped in the 3900 BP–4100 BP period, clearly separated from samples of the types B and C.

Although, obviously, a more extensive set of samples would be necessary for testing the above considerations, the above data suggest that electrochemical data can complement and be correlated to chemical composition and isotope ratios for grouping of metal samples yielding information of archaeological value regarding the provenance of raw material and the characteristics of the manufacturing process.

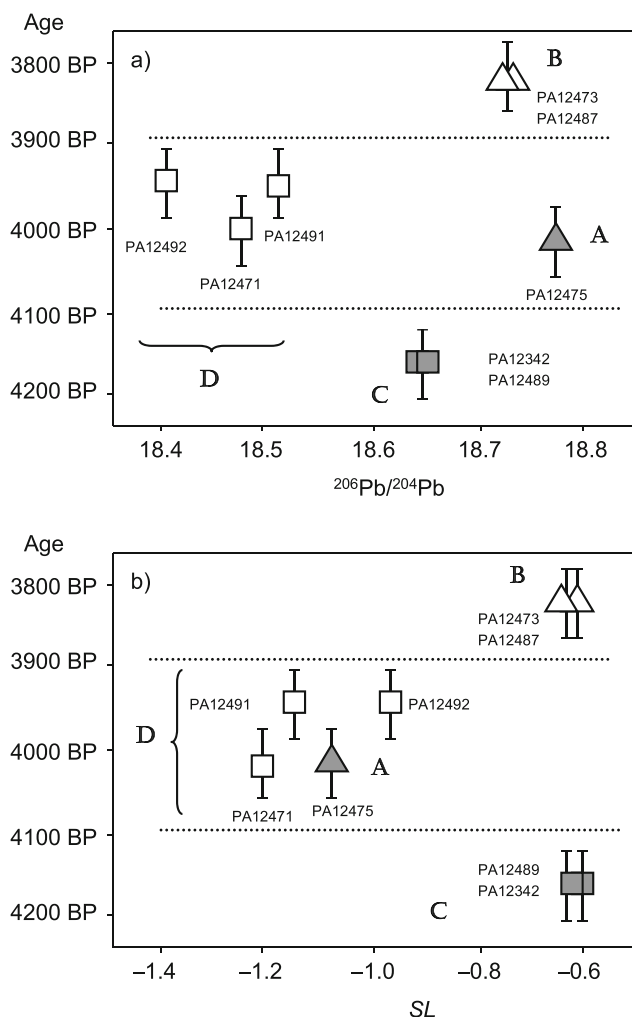


Fig. 9 Chronological variation of **a** the $^{209}\text{Pb}/^{204}\text{Pb}$ isotope ratio (data from ref. [44]), and **b** the slope of the $\log[i(C_{Cu2})/i(C_{Cu1})]$ vs. $\log i(C_{Cu1})$ linear representations for La Vital samples in this study. Radiocarbon ages from ref. [45]

Conclusions

Voltammetric data for submicrosamples from the corrosion layers of copper artifacts from the archaeological site of La Vital (Gandia, Spain), of particular interest as presenting the first evidences for copper metallurgy in the Iberian Peninsula, can be used for grouping it. The variation of the intensities of the voltammetric signals corresponding to the reduction of cuprite plus malachite and tenorite recorded upon attachment of samples to graphite electrodes in contact with aqueous acetate buffer at pH 4.50 can be modeled assuming the presence of concentration gradients of the different corrosion products in the secondary patina governed by potential rate laws. These voltammetric features considered as sensitive to both the provenance of the raw materials and the type of manufacturing process. Electrochemical grouping can be correlated satisfactorily with provenances derived from independent available data on lead isotope and chemical composition analyses.

Funding information This study received financial support from the project CTQ2017-85317-C2-1-P, supported with *Ministerio de Economía, Industria y Competitividad* (MINECO), *Fondo Europeo de Desarrollo Regional* (ERDF), and *Agencia Estatal de Investigación* (AEI).

References

- Radivojevic M, Rehren T, Pernicka E, Silvar D, Brauns M, Boric D (2010) On the origin of extractive metallurgy: new evidence from Europe. *J Archaeol Sci* 37:2775–2787
- Sessa C, Bagán H, Romero MT, García JF (2017) Effects of variability sources on analysis of the composition of large ancient metal objects. *Microchem J* 134:309–316
- Constantinides I, Gritsch M, Adriaens A, Hutter H, Adams F (2001) Microstructural characterisation of five simulated archaeological copper alloys using light microscopy, scanning electron microscopy, energy dispersive X-ray microanalysis and secondary ion mass spectrometry. *Anal Chim Acta* 440:189–198
- Shalev S, Shilstein SS, Yekutieli Y (2006) XRF study of archaeological and metallurgical material from an ancient copper-smelting site near Ein-Yahav, Israel. *Talanta* 70:909–913
- Gaudiuso R, Dell’Aglia M, De Pascale O, Loperfido S, Mangone A, De Giacomo A (2014) Laser-induced breakdown spectroscopy of archaeological findings with calibration-free inverse method: comparison with classical laser-induced breakdown spectroscopy and conventional techniques. *Anal Chim Acta* 813:15–24
- del Hoyo-Meléndez JM, Swit P, Matosz M, Wozniak M, Klisinska-Topacz A, Bratasz L (2015) Micro-XRF analysis of silver coins from medieval Poland. *Nucl Inst Methods Phys Res B* 349:6–16
- Gale NH, Stos-Gale ZA, Malotis G, Annetts N (1997) Lead isotope data from the isotrace laboratory, Oxford: Archaeometry data base 4, ores from Cyprus. *Archaeometry* 39:237–246
- Attanasio D, Bultrini G, Ingo GM (2001) The possibility of provenancing a series of bronze punic coins found at Tharros (Western Sardinia) using the literature lead isotope database. *Archaeometry* 43:529–547
- Resano M, Marzo MP, Alloza R, Saénz C, Vanhaecke F, Yang L, Willie S, Sturgeon RE (2010) Laser ablation single-collector inductively coupled plasma mass spectrometry for lead isotopic analysis to investigate evolution of the Bilbilis mint. *Anal Chim Acta* 677:55–63
- Gomes SS, Monge Soares A, Araujo MF, Correia VH (2016) Lead isotopes and elemental composition of Roman fistulae plumbeae aquariae from Conimbriga (Portugal) using Quadrupole ICP-MS. *Microchem J* 129:184–193
- Klein S, Lahaye Y, Brey GP (2004) The Early Roman Imperial AES coinage II: tracing the copper sources by analysis of lead and copper isotopes-copper coins of Augustus and Tiberius. *Archaeometry* 46:469–480
- Balliana E, Aramendía M, Resano M, Barbante C, Vanhaecke F (2013) Copper and tin isotopic analysis of ancient bronzes for archaeological investigation: development and validation of a suitable analytical methodology. *Anal Bioanal Chem* 405:2973–2986
- Scott DA (1994) An examination of the patina and corrosion morphology of some Roman bronzes. *J Am Inst Cons* 33:1–23
- Robbiola L, Blengino J-M, Fiaud C (1998) Morphology and mechanisms of formation of natural patinas on archaeological CuSn alloys. *Corros Sci* 40:2083–2111
- Agresti J, Osticioli I, Guidotti MC, Kardjilov N, Siano S (2016) Non-invasive archaeometallurgical approach to the investigations of bronze figurines using neutron, laser, and X-ray techniques. *Microchem J* 124:765–774
- Robbiola L, Portier R (2006) A global approach to the authentication of ancient bronzes based on the characterization of the alloy-patina-environment system. *J Cult Herit* 7:1–12
- Chiavari C, Rahmouni K, Takenouti H, Joiret S, Vermaut P, Robbiola L (2007) Composition and electrochemical properties of natural patinas of outdoor bronze monuments. *Electrochim Acta* 52:7760–7769
- Scholz F, Meyer B (1998) Voltammetry of solid microparticles immobilized on electrode surfaces. In: Bard AJ, Rubinstein I (eds) *Electroanalytical chemistry, a series of advances*, vol 20. Marcel Dekker, New York, pp 1–86
- Scholz F, Schröder U, Gulabowski R, Doménech-Carbó A (2014) *Electrochemistry of immobilized particles and droplets*, 2nd. Springer, Berlin-Heidelberg
- Doménech-Carbó A, Labuda J, Scholz F (2013) *Electroanalytical chemistry for the analysis of solids: characterization and classification* (IUPAC Technical Report). *Pure Appl Chem* 85:609–631
- Costa V, Leyssens K, Adriaens A, Richard N, Scholz F (2010) Electrochemistry reveals archaeological materials. *J Solid State Electrochem* 14:449–451
- Arjmand F, Adriaens A (2012) Electrochemical quantification of copper-based alloys using voltammetry of microparticles: optimization of the experimental conditions. *J Solid State Electrochem* 16:535–543
- Serghini-Idrissi M, Bernard MC, Harif FZ, Joiret S, Rahmouni K, Srhiri A, Takenouti H, Vivier V, Ziani M (2005) Electrochemical and spectroscopic characterizations of patinas formed on an archaeological bronze coin. *Electrochim Acta* 50:4699–4709
- Doménech-Carbó A, Doménech-Carbó MT, Martínez-Lázaro I (2008) Electrochemical identification of bronze corrosion products in archaeological artifacts, a case study. *Microchim Acta* 162:351–359
- Satovic D, Martinez S, Bobrowski A (2010) Electrochemical identification of corrosion products on historical and archaeological bronzes using the voltammetry of micro-particles attached to a carbon paste electrode. *Talanta* 81:1760–1765
- Doménech-Carbó A, Doménech-Carbó MT, Costa V (2009) In: Scholz F (ed) *Electrochemical methods in archaeometry, conservation and restoration*, Monographs in Electrochemistry Series. Springer, Berlin-Heidelberg
- Doménech-Carbó A (2010) Voltammetric methods applied to identification, speciation and quantification of analytes from works of art: an overview. *J Solid State Electrochem* 14:363–379
- Doménech-Carbó A, Doménech-Carbó MT (2018) *Electroanalytical techniques in archaeological and art conservation*. *Pure Appl Chem* 90:447–462
- Doménech-Carbó A (2017) Electrochemical dating: a review. *J Solid State Electrochem* 21:1987–1998
- Capelo S, Homem PM, Cavalheiro J, Fonseca ITE (2013) Linear sweep voltammetry: a cheap and powerful technique for the identification of the silver tarnish layer constituent. *J Solid State Electrochem* 17:223–234
- Cepriá G, Abadías O, Pérez-Arantegui J, Castillo JR (2001) Electrochemical behavior of silver-copper alloys in voltammetry of microparticles: a simple method for screening purposes. *Electroanalysis* 13:477–483
- Doménech-Carbó A, Del Hoyo-Menéndez J, Doménech-Carbó MT, Piquero-Cilla J (2017) Electrochemical analysis of the first Polish coins using the voltammetry of immobilized particles. *Microchem J* 130:47–55
- Di Turo F, Montoya N, Piquero-Cilla J, De Vito C, Coletti F, Favero G, Doménech-Carbó A (2017) Archaeometric analysis of Roman bronze coins from the *Magna Mater* temple using solid-state voltammetry and electrochemical impedance spectroscopy. *Anal Chim Acta* 955:36–47

34. Doménech-Carbó A, Doménech-Carbó MT, Montagna E, Lee Y (2017) Electrochemical discrimination of mints: the last Chinese emperors Kuang Hsü and Hsüan T'ung monetary unification. *Talanta* 169:50–56
35. Doménech-Carbó A, Doménech-Carbó MT, Álvarez-Romero C, Montoya N, Pasies-Oviedo T, Buendía M (2017) Electrochemical characterization of coinage techniques the 17th century: the maravedis case. *Electroanalysis* 29:2008–2018
36. Di Turo F, Montoya N, Piquero-Cilla J, De Vito C, Coletti F, Favero G, Doménech-Carbó MT, Doménech-Carbó A (2018) Dating archaeological strata in the *Magna Mater* Temple using solid-state voltammetric analysis of leaded bronze coins. *Electroanalysis* 30: 361–370
37. Doménech-Carbó A, Doménech-Carbó M T, Capelo S, Pasies-Oviedo T, Martínez-Lázaro I (2014) Dating archaeological copper/bronze artifacts using the voltammetry of microparticles. *Angew Chem Int Ed* 53:9262–9266
38. Doménech-Carbó A, Doménech-Carbó MT, Redondo-Marugán J, Osete-Cortina L, Barrio J, Fuentes A, Vivancos-Ramón MV, Al-Sekhaneh W, Martínez B, Martínez-Lázaro I, Pasies-Oviedo T (2018) Electrochemical characterization and dating of archeological leaded bronze objects using the voltammetry of immobilized particles. *Archaeometry* 60:308–324
39. Doménech-Carbó A, Doménech-Carbó MT, Peiró-Ronda MA (2011) Dating archaeological lead artifacts from measurement of the corrosion content using the voltammetry of microparticles. *Anal Chem* 83:5639–5644
40. Ferragud-Adam X, Piquero-Cilla J, Doménech-Carbó MT, Guerola-Blay V, Company X, Doménech-Carbó A (2017) Electrochemical analysis of gildings in Valencia Altarpieces: a cross-age study since 15th until 20th century. *J Solid State Electrochem* 21:1477–1487
41. Martínez B, Piquero-Cilla J, Montoya N, Doménech-Carbó MT, Doménech-Carbó A (2018) Electrochemical analysis of gold embroidery threads from archaeological textiles. *J Solid State Electrochem* 22:2205–2215
42. Doménech-Carbó A, Scholz F, Doménech-Carbó MT, Piquero-Cilla J, Montoya N, Pasies-Oviedo T, Gozalbes M, Melchor-Montserrat JM, Oliver A (2018) Dating of archaeological gold by means of solid state electrochemistry. *ChemElectroChem* 5:2113–2117
43. Doménech-Carbó A, Scholz F (2019) Electrochemical age determinations of metallic specimens – *the utilization of the corrosion clock*. *Acc Chem Res* 52:400–406
44. Doménech-Carbó A, Doménech-Carbó MT, Peiró-Ronda MA, Martínez-Lázaro I, Barrio J (2012) Application of the voltammetry of microparticles for dating archaeological lead using polarization curves and electrochemical impedance spectroscopy. *J Solid State Electrochem* 16:2349–2356
45. Doménech-Carbó A, Lastras M, Rodríguez F, Cano E, Piquero-Cilla J, Osete-Cortina L (2014) Monitoring stabilizing procedures of archaeological iron using electrochemical impedance spectroscopy. *J Solid State Electrochem* 18:399–409
46. Di Turo F, Parra R, Piquero-Cilla J, Favero G, Doménech-Carbó A (2019) Crossing VIMP and EIS for studying heterogeneous sets of copper/bronze coins. *J Solid State Electrochem* 23:771–781
47. Rovira S, Montero-Ruiz E (2011) Aspectos metalúrgicos, in Pérez-Jordá G, Bernabeu-Aubán J, Carrión-Marco Y, García-Puchol O, Molina-Balaguer L, Gómez-Puche M, La Vital (Gandia, Valencia): vida y muerte en la desembocadura del Serpis durante el III y el I milenio a.C. Museo de Prehistoria de Valencia, Valencia, pp. 219–227
48. Díaz-Castillo A (2011) El marco cronológico a partir de la evidencia radiocarbónica del yacimiento de La Vital, in Pérez-Jordá G, Bernabeu-Aubán J, Carrión-Marco Y, García-Puchol O, Molina-Balaguer L, Gómez-Puche M, Eds. La Vital (Gandia, Valencia): vida y muerte en la desembocadura del Serpis durante el III y el I milenio a.C. Museo de Prehistoria de Valencia, Valencia, pp. 235–245
49. Budd P, Gale D, Pollard AM, Thomas RG, Williams PA (1993) Evaluating lead isotope data: further observations. *Archaeometry* 35:241–247
50. Budd P, Pollard AM, Scaiffé B, Thomas RG (1995) The possible fractionation of lead isotopes in ancient metallurgical processes. *Archaeometry* 37:143–150
51. Baron S, Le-Carlier C, Carignan J, Ploquin A (200) Archaeological reconstruction of medieval lead production: implications for ancient metal provenance studies and paleopollution tracing by Pb isotopes. *Appl Geochem* 24:2093–2101
52. Burgio L, Clark RJH (2001) Library of FT-Raman spectra of pigments, minerals, pigment media and varnishes, and supplement to existing library of Raman spectra of pigments with visible excitation. *Spectrochim Acta A* 57:1491–1521
53. Caggiani MC, Cosentino A, Mangone A (2016) Pigments Checker version 3.0, a handy set for conservation scientists: a free online Raman spectra database. *Microchem J* 129:123–132
54. Stos-Gale Z, Gale NH, Houghton J, Speakman R (1995) Lead isotope data from the isotrace laboratory, Oxford: Archaeometry data base 1, ores from the Western Mediterranean. *Archaeometry* 37: 407–415
55. Kuleff I, Iliev I, Pernicka E, Gergova D (2006) Chemical and lead isotope compositions of lead artifacts from ancient Thracia (Bulgaria). *J Cult Herit* 7:244–256
56. Doménech-Carbó A, Doménech-Carbó MT, Redondo-Marugán J, Osete-Cortina L, Vivancos-Ramón MV (2016) Electrochemical characterization of corrosion products in leaded bronze sculptures considering ohmic drop effects on Tafel analysis. *Electroanalysis* 28:833–845
57. Scott DA (1997) Copper compounds in metals and colorants: oxides and hydroxides. *Stud Conserv* 42:93–100

Publisher's note Springer Nature remains neutral with regard to jurisdictional claims in published maps and institutional affiliations.